USING MULTI-SHELL PHASE CHANGE MATERIALS LAYERS FOR COOLING A LITHIUM-ION BATTERY

by

Ramin NASEHI, Arghavan ALAMATSAZ, and Mohammad Reza SALIMPOUR*

Department of Mechanical Engineering, Isfahan University of Technology, Isfahan, Iran

Original scientific paper
DOI: 10.2298/TSCI130515033N

One of the cooling methods in engineering systems is usage of phase change materials. Phase change materials which have high latent heats, are usually used where high energy absorption in a constant temperature is required. This work presents a numerical analysis of phase change materials effects on cooling lithium-ion batteries and their decrease in temperature levels during intense discharge. In this study, three phase change materials shells with different thermophysical specifications located around a battery pack are examined. The results of each possible arrangement are compared together, and the best arrangement leading to the lowest battery temperature during discharge is identified. In addition, the recovery time for the system which is the time required for the change materials to refreeze is investigated.

Key words: *phase change materials, lithium-ion battery, liquid fraction, thermal management systems, cooling, recovery*

Introduction

Due to their high energy storage ability, lithium-ion (Li-ion) batteries have various applications in industry. Some noteworthy characteristics of these batteries are their long life cycle, relatively low cost, and low discharge. These kinds of batteries are extensively used in electronic devices such as cell phones and laptops.

Li-ion batteries provide high energy density at a low price, but they are limited in application because of their excessive heat generation rate coupled with an adverse effect of temperature on battery life [1]. Consequently, controlling battery temperature rise is one of the manufacturer's concerns.

Controlling the temperature of systems has always been one of the engineers' concerns and thus a lot of researches have been devoted on this field. Hajmohammadi *et al.* [2] documented two reliable methods to cope with the rising temperature in an array of heated segments based on minimization of the hot spot in the array. They showed that their methods can considerably reduce the hot spot temperatures. In another work Hajmohammadi *et al.* [3] used conductive thick plate as a heat transfer interface between the heat source and the cold flowing fluid and studied its' advantages and disadvantages. They proved that there exists an optimal thickness of the thick plate, which minimizes the peak temperature.

* Corresponding author; e-mail: salimpour@cc.iut.ac.ir

Various systems are designed and manufactured to control batteries maximum temperature during charge and discharge periods. Air cooling systems with fans and passive thermal management systems using phase change materials (PCM), are the most important ones. An air cooling system with an electronic fan is not an attractive way due to its bulkiness and additional power requirement. On the other hand, using PCM for cooling batteries seems to be a preferable way.

Different thermal management systems have been investigated numerically and experimentally. Radhakrishnan and Balakrishnan [4] studied the effect of presence of PCM in a pipe with the heat transfer fluid flowing in the annulus. In a work done by Kurklu *et al.* [5], a mathematical model was developed for the prediction of the thermal performance of a PCM store containing a polypropylene tube. Domanski and Fellah [6] evaluated the performance of phase-change, thermal-energy storage unites from the second-law view point.

A thorough literature investigation into the use of PCM for energy saving and management in green house was carried out in the work done by Kurklu [7]. Zivkovic and Fujii [8] developed a simple computational model for isothermal phase change of PCM encapsulated in a single container. In this research, a mathematical model was presented based on enthalpy formulation for rectangular and cylindrical containers. They used numerical analysis and concluded that the rectangular container required nearly half of the melting time compared with the cylindrical container of the same volume and heat transfer area. Enibe [9] applied PCM in a system for crop drying and poultry egg incubation. He tested the system experimentally and showed that it could be operated successfully for that purpose. Mahfuz *et al.* [10] performed an exergy analysis of a solar thermal power system with PCM storage.

Al-Hallaj and Selman [11] made and tested a prototype of a PCM-based system as a passive cooling system for Li-ion batteries used in EV/HEV. They concluded that this system could be a suitable substitute for active cooling systems without complicating or adding any moving component to the system. In another work done by Al-Hallaj and Selman [12], it was observed that using PCM in batteries caused the uniformity of temperature profile during discharge. Alawadhi and Amon [13] examined the effectiveness of a PCM and thermal control element for portable devices and found out that the geometry and size of thermal control element have profound effects on the battery temperature. To overcome the low thermal conductivity of the PCM and low natural convection heat transfer coefficient, Khateeb *et al.* [14] invoked aluminum foam within the PCM and attached foam to battery module.

Ramandi *et al.* [15] assumed two PCM layers with different materials around the battery, considering its effect on cooling the battery. They investigated thermal conductivity and melting point as two effective parameters and showed that different PCM arrangements affect the maximum temperature of the battery. They also used the results to analyze the exergy losses by considering heat transfer inside the battery and PCM.

Going through the literature, it was observed that putting multiple (more than two) layers of PCM around the Li-ion batteries has not been investigated, yet. Therefore, in the present study, this case was simulated and the effects of different parameters on the battery temperature were studied. Another important notion of the present study is the investigation of PCM layers during recovery mode, *i. e.* when heat is removed from PCM.

Battery module design

Li-ion battery cells are manufactured in various shapes such as rectangular and cylindrical. In this study, a battery which is formed from 100 cylindrical cells with commercial

name of 2.2Ah-18650 is considered. The properties of this battery are used throughout the present work.

Mills and Al-Hallaj [1] simulated a battery consisting of 2.2Ah-18650 cells and also derived experimental data. They reported the heat generation for a commercial 2.2Ah-18650 Li-ion battery in different discharge rates. Using this report, 0.0982 Wh was selected to calculate the heat generation rate.

As previously mentioned, the battery consists of one hundred 2.2Ah-18650 cells, hence the dimensions of the battery would be 0.09 m × 0.18 m × 0.13 m, which are obtained by putting two plates with 50 cells on top of each other (each plate consists of 10 × 5 cells).

In this paper, six possible arrangements for three PCM layers around the battery are examined and the results have been compared with the single PCM layer. It must be noted that the PCM mass in each layer is considered fixed while the PCM mass in single layer battery is assumed to be the sum of PCM masses of three layers.

Problem geometry

As the variations of different parameters in the z-direction are negligible, a 2-D geometry is considered in this study. This geometry consists of a rectangular domain with internal heat generation that represents the battery. Around the rectangular domain (except the bottom surface) there are PCM layers. Thus, for the single layer case, one PCM layer and for the multi-layer cases, three PCM layers are placed around the domain. Hence, a thin aluminum sheet resides between each of the two successive layers. The reason for selecting aluminum is its lightness and high thermal conductivity. The geometry of the problem is illustrated schematically in fig. 1.

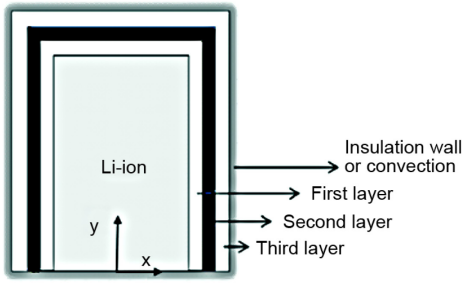

Figure 1. Problem geometry

Table 1 represents the thermo-physical properties of PCM used in this study, respectively. Thermal conductivity, heat capacity and density of battery are 3 W/mK, 0.89 kJ/kgK, and 2670 kg/m^3, respectively, while these parameters for battery pack are 0.2 W/mK, 1.8 kJ/kgK, and 1210 kg/m^3, respectively.

Table 1. The PCM thermo-physical properties

PCM Number	1	2	3
PCM name	Capric Acid	Eicosane	$Na_2(SO_4)\cdot 10H_2O$
Melting temperature, [K]	304.5	309.8	305.4
Latent heat, [kJkg^{-1}]	153	241	254
Density, [kgm^{-3}]	884	778	1485
Thermal conductivity, [Wm^{-1}K^{-1}]	2	0.27	0.544
Specific heat for liquid phase, [Jkg^{-1}K^{-1}]	2761	2350	3349
Specific heat for solid phase, [Jkg^{-1}K^{-1}]	2096	2132	2093

The type of PCM and their thicknesses used in each layer of possible arrangements and also for the single layer are given in tab. 2. For later usages, the six different arrange-

ments are named A, B, C, D, E, and F. The given thicknesses are based on the assumption that PCM masses are equal in each layer.

Table 2. Types of PCM and their thicknesses used in each possible layer of arrangements and for the single layer

		First layer	Second layer	Third layer
A	Material	PCM1	PCM 2	PCM 3
	Thickness, [mm]	5	4.4	2.8
B	Material	PCM 1	PCM 3	PCM 2
	Thickness, [mm]	5	2.9	4.3
C	Material	PCM 2	PCM 1	PCM 3
	Thickness, [mm]	4.3	4.8	2.8
D	Material	PCM 2	PCM 3	PCM 1
	Thickness, [mm]	4.6	2.9	4.6
E	Material	PCM 3	PCM 1	PCM 2
	Thickness, [mm]	3.1	4.8	4.3
F	Material	PCM 3	PCM 2	PCM 1
	Thickness, [mm]	3.1	4.5	4.6
Single layer	Material	PCM 1	–	–
	Thickness, [mm]	14.3	–	–

Numerical simulations

Solution method

One of the problems in numerical simulation of PCM is the track of the moving interface. Although for simple geometries, analytical solution may be achieved, in more applied cases where the geometries are more complicated the enthalpy form of the energy balance should be used. In this method, the energy equation is incorporated in both phases. One of the techniques used for modeling melting process is enthalpy porosity scheme. In this method, liquid fraction of each cell of the domain shall be calculated based on enthalpy balance.

Moreover, to take into account the pressure drop caused by the presence of the solid material, appropriate sink terms are added to the momentum equations. The region in which liquid fraction resides between zero and one is called mushy zone. If in a cell, PCM is fully melted, its porosity will be one.

The following assumptions were considered in the present analysis.

The battery discharge rate is constant, hence the heat generation inside the battery is assumed to be steady. The fluid flow (for melting PCM) is laminar and the fluid is considered Newtonian. The radiation heat transfer was neglected and thermo-physical properties of PCM (except C_p) were assumed to be constant.

Based on the assumptions, the governing equations and definitions on PCM are obtained:

The PCM enthalpy is $H = h + \Delta H$ where $h = h_{\text{ref}} + \int_{T_{\text{ref}}}^{T} C_p \mathrm{d}T$. Liquid fraction, β, equals to zero when $T < T_m$ and is unity otherwise. Therefore, the required energy for phase change is $\Delta H = \beta L$.

Hence, the energy, mass, and momentum conservation equations can be written:

$$\frac{\partial}{\partial t}(\rho H) + \nabla(\rho \vec{\mathrm{v}} H) = \nabla(k\Delta T) + S_{\mathrm{h}} \tag{1}$$

$$\frac{\partial \rho}{\partial t} + \nabla(\rho \vec{\mathrm{v}}) = 0 \tag{2}$$

$$\frac{\partial}{\partial \mathrm{t}}(\rho \vec{\mathrm{v}}) + \nabla(\rho \vec{\mathrm{v}} \vec{\mathrm{v}}) = -\nabla P + \nabla \boldsymbol{\tau} + \rho \vec{\mathrm{g}} + S_{\mathrm{m}} \tag{3}$$

where

$$S_{\mathrm{m}} = \frac{1-\beta^2}{\beta^3 + \varepsilon} A_{\mathrm{mush}}(\vec{\mathrm{v}} - \vec{\mathrm{v}}_{\mathrm{p}}), \qquad \nabla^2 \vec{\mathrm{v}}_{\mathrm{p}} = 0, \qquad \text{and} \qquad \boldsymbol{\tau} = \mu\left[(\nabla \vec{\mathrm{v}} + \nabla \vec{\mathrm{v}}^T) - \frac{2}{3}\nabla \vec{\mathrm{v}} \mathbf{I}\right]$$

Inside the battery, the energy conservation equation will be:

$$\frac{\partial}{\partial t}(\rho H) = \nabla(k\Delta T) + S_{\mathrm{h}} \tag{4}$$

In this paper, control volume method with double precision is used for problem solution. For energy and momentum equations, second order upwind discretization scheme, and for time first order discretization are chosen. The initial temperature for PCM and the battery is considered 303 K. Using these initial values and the following boundary conditions, the problem was solved, transiently.

Boundary conditions

Two types of boundary conditions at the outer walls were considered: insulated walls and convection heat transfer at the walls.

Insulated walls

Boundary condition equations at vertical and horizontal outer walls are $\partial T/\partial x = 0$ and $\partial T/\partial y = 0$, respectively. The interface between first and second layers, second and third layers and also battery's wall and first layer are coupled, consequently the temperature of both sides will be equal.

Convection heat transfer at walls

Boundary condition equations for vertical and horizontal outer walls are:

$$-k\frac{\partial T}{\partial x} = h(T_{\mathrm{w}} - T_{\mathrm{amb}}) \tag{5}$$

$$-k\frac{\partial T}{\partial y} = h(T_{\mathrm{w}} - T_{\mathrm{amb}}) \tag{6}$$

Mesh and time step independency study

In order to show time step and grid size independency, first the magnitude of the time step was changed and the results were compared. The independency of maximum temperature inside the battery and liquid fraction upon time are examined for a grid with 124631 cells. It was seen that the results agree closely with each other; and hence time step size independency could be concluded for this grid size and time step 0.2 s.

In the next stage, to investigate grid size independency for time step 0.2 s, simulations for grids with 61534, 124631, and 181406 number of cells were repeated. From the results, it was concluded that a grid with 124631 cells and time step 0.2 s is appropriate.

Validation

To validate the present solution, the results of a case reported in [16] were reproduced. The problem of [16] consists of a rectangular domain within which PCM is placed. Three sides of this domain are insulated and the forth side is kept at a constant temperature. The temperature of forth side is T_o and initial temperature for whole domain is set at T_i. Parameter b indicates the distance of solid-liquid interface from y-axis. This parameter is defined as $T_p(x_b, t) = T_m$ where $x_b = b$.

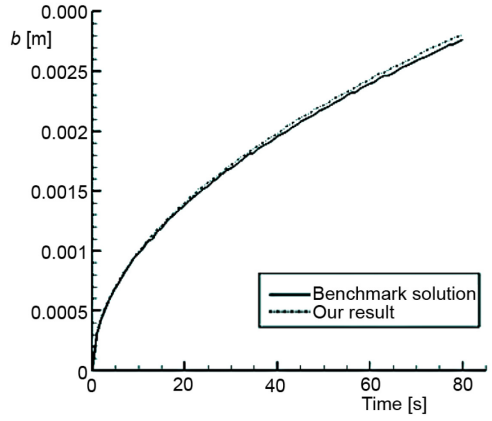

Figure 2. Validation model result

Figure 2 shows the results of the present numerical simulation and Benchmark solution [16]. As it can be seen these results are consistent. Therefore, this numerical model can be used to solve the upcoming problems.

Results and discussion

Effect of specific heats of phases

In different studies about PCM simulations it is common to assume the same value of specific heat for both liquid and solid phases. However, in this study before doing the simulations, the level of reasonability of this assumption is investigated. To do so, first specific heat for both liquid and solid phases of PCM1 was considered 2090 J/kgK. Then, the specific heats of solid phase and liquid phase were assumed to be 2090 J/kgK and 2761 J/kgK, respectively. From the results, it was seen that using different values for specific heats of different phases does not cause a remarkable effect in results.

Results for insulated boundary condition

The graph shown in fig. 3 illustrates the maximum temperature inside the battery as a function of time during 7200 s. Based on these results, the maximum temperature inside the battery ranges from 313-317 K for different PCM arrangements. Among all possible arrangements, cases B and E have minimum temperature.

In addition, the single layer seems to have the best result. The minimum temperature of single layer is due to two reasons.

(1) Among all used PCM (in use), PCM1 has the maximum thermal conductivity and since PCM1 has been used for the single layer, heat resistance in the heat transfer path is lower than other arrangements.

(2) The PCM1 has the lowest melting temperature, thus it starts melting earlier.

As is seen in fig. 3, all the arrangements except cases A and F experience a similar uniform trend. The excepted cases A and F experience a sudden slope change in 4000^{th} and 5500^{th} seconds, respectively. The slopes in the graph represent the rate of temperature increase.

Figure 4 plots the changes in liquid fraction as a function of time for case A. As is seen, at first the liquid fraction for all three layers is zero, however, after a while with heat generation inside the battery the temperature rises, and about 800 s after the start of discharge, the first PCM layer starts melting. As time passes, the liquid fraction in the first layer rises and at the same time the temperature of the second and third layers increases until 3650th second that the third layer starts melting as well. After 5000 s all PCM in the first layer is melted. Consequently, phase change begins in the second layer after 6700 s. The order of PCM layers melting depends on their melting points and the distance between battery center and the layers. The first layer contains PCM1 which has the lowest melting point (304.5 K), thus phase change begins within the first layer. In the second layer PCM2 with melting point of 309.8 K and in the third layer PCM3 with melting point of 305.4 K are placed. Hence in the third layer, despite its longer distance from battery center, melting commences earlier.

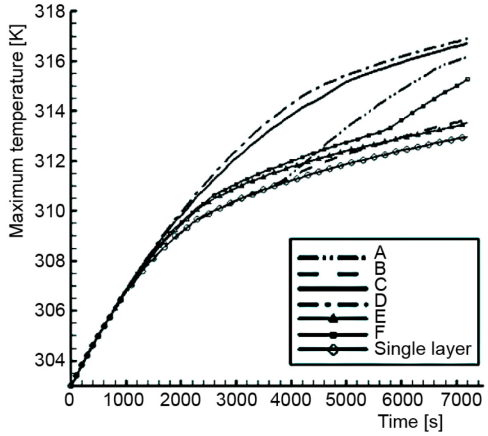

Figure 3. Maximum temperature trends for different PCM arrangements

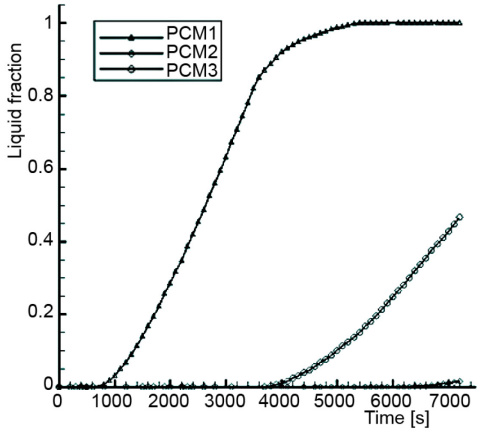

Figure 4. Liquid fraction as a function of time for arrangement A after 7200 s

In fig. 3, the maximum temperature graph witnesses a sudden slop change for arrangement A in 4000th second. This can be justified by regarding to the liquid fraction graph; in 4000th second for the same arrangement (A), liquid fraction rate in the first layer decreases dramatically that the increasing rate in the third layer cannot compensate it. The result is an increase in the battery temperature rise. However, by increasing the liquid fraction rate in the third layer, the temperature rise declines gradually. The reason for time delay in liquid fraction increasing rate of the third layer is the presence of PCM2 in the second layer. Since, PCM2 has the lowest thermal conductivity in comparison with other PCM, (for a higher heat transfer) it needs a larger temperature difference which is provided by the battery temperature rise.

The changes in liquid fraction for arrangement B during 7200 s is plotted in fig. 5. In this case, the order of melting is different (and the third layer does not melt at all). The first layer melting initiates after 800 s and it turns completely to liquid after 5000 s. The second layer begins melting in the 3600th second and finally its liquid fraction reaches 0.7.

As mentioned previously, arrangement B is the best case. The underlying reason is that in this case PCM2 is placed in the third layer. According to tab. 1, PCM2 has the lowest thermal conductivity and the highest melting point and slowly allows heat to pass within it, hence phase change happens slower.

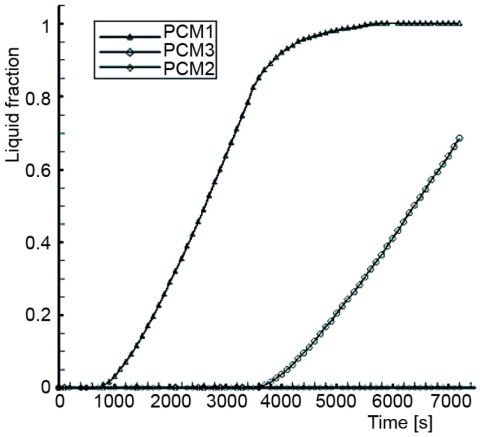

Figure 5. Liquid fraction as a function of time, for arrangement B after 7200 s

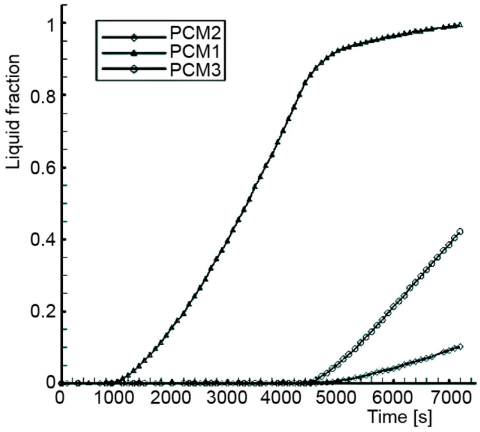

Figure 6. Liquid fraction as a function of time, for case C after 7200 s

Presented in fig. 6, are liquid fraction graphs after 7200 s for case C. The liquid fraction variations of all three layers are shown in the graph. It states that in this case melting initiates firstly in the second layer containing PCM1 in 900th second, which is due to the PCM1 comparatively lower melting point. After that, in the 4500th second the third layer constituted of PCM3 starts phase changing and eventually in the 5000th second, PCM2 in the first layer begins to melt. After 7200 s the liquid fraction amounts of the first, second and third layer are equal to 0.1025, 0.9946, and 0.4209, respectively. In this case unlike the two previous cases, PCM1 does not melt completely and this is because it is located in the second layer and receives energy with a time delay.

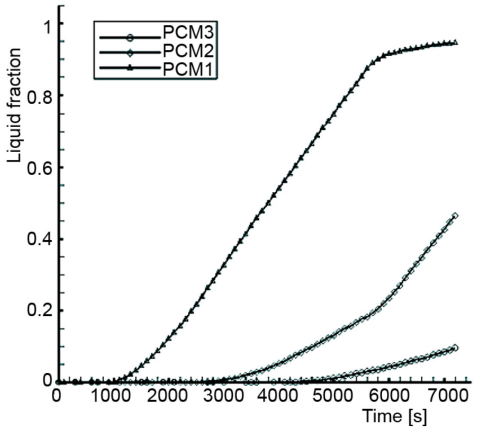

Figure 7. Liquid fraction as a function of time, for arrangement D after 7200 s

As is seen in fig. 6, in case C the maximum battery temperature after 7200 s is 316.7 K which is not favorable in comparison with other cases. This is because of PCM2 location in first layer. Since PCM2 has the lowest thermal conductivity among the used PCM (*i. e.* high thermal resistance) and there is less heat transfer, a higher temperature difference is required which is compensated by the battery temperature rise.

The graph in fig. 7 illustrates the variations of liquid fraction of case D. The melting order of layers is the third, the second and the first layer and after two hours from the start of discharge, the liquid fraction of PCM layers are 0.0945, 0.4662, and 0.9479, respectively. This time again PCM2 is located in the first layer and it plays the role of a barrier for heat transfer from the battery to the other layers. The hot spot after two hours in this case is 316.9 K. This temperature is higher than other cases and explains why case D is not a good choice to control the battery temperature rise.

Figure 7 discloses that in the 5700th second a sadden slop change occurs in the second layer which is accompanied by increase of liquid fraction rate. This is because of the

sharp and sudden decrease in the third layer's liquid fraction rate, since in the 5200th second a large proportion of the third layer's PCM is melted.

Liquid fraction as a function of time after 7200 s, for case E is given in fig. 8. This figure reveals that the liquid fraction of the third PCM layer which contains PCM2 does not change up to two hours. The second layer containing PCM1 starts melting in the 900th second while in 1800th second, melting of the first layer containing PCM3 begins. In this case, the maximum temperature inside the battery after 7200 s is 313.5 K which is the minimum temperature among all the six cases, *i. e.* case E is paramount.

Plotted in fig. 9 are liquid fraction variations with time and its contour after two hours for case F. In this case unlike cases B and E, the second layer has a liquid fraction of zero. It is obvious that the reason is the placement of PCM2 in this layer. The first and the third layers both start melting at the 1000th second. The battery maximum temperature rises up to 315.3 K since PCM2 is placed between the first and third layers, and hence it plays the role of a heat resistance and hinders heat transfer.

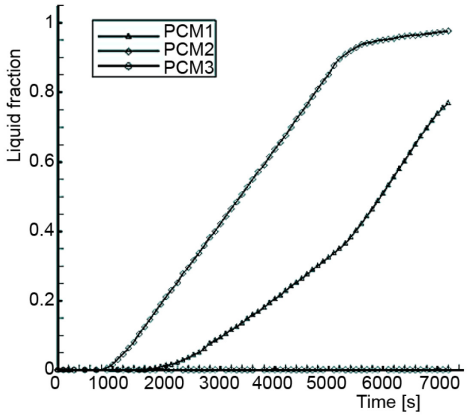

Figure 8. Liquid fraction as a function of time, for arrangement E after 7200 s

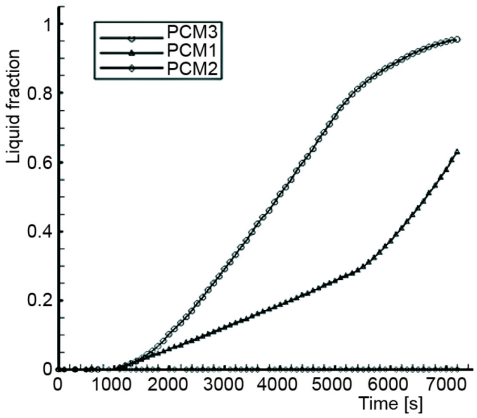

Figure 9. Liquid fraction as a function of time, for arrangement F after 7200 s

A summary of the results for all possible PCM combinations with insulated outer wall as the boundary condition is given in tab. 3. According to these data, the single layer has

Table 3. The summary of results after 7200 s for system with insulated walls

	Liquid fraction of PCM1	Liquid fraction of PCM2	Liquid fraction of PCM3	Total liquid fraction	Maximum temperature [K]
A: 1,2,3	1	0.0160	0.4672	0.4944	315.798
B: 1,3,2	1	0	0.6854	0.5618	313.672
C: 2,1,3	0.9946	0.1025	0.4209	0.5060	316.711
D: 2,3,1	0.9479	0.0945	0.4662	0.5029	316.879
E: 3,1,2	0.9759	0	0.7688	0.5816	313.527
F: 3,2,1	0.6310	0	0.9560	0.5290	315.259
Single layer	0.7619	0	0	0.7619	312.971

the least hot spot. However, if PCM systems with three layers with insulated walls are to be used, the best choices would be cases B and E. In fact, in multiple PCM shell the most effective options is the one in which the PCM with low thermal conductivity and high melting temperature is located in the outermost layer.

Results for convection heat transfer in the outermost walls

As observed in the previous simulation with insulated walls, case E had the best result, D had the worst and the single layer performed better than the multi-shell systems. Therefore, this time only these three cases were selected to be simulated with a new boundary condition *i. e.* convection heat transfer in the outermost walls. Figure 10 represents the battery maximum temperature for these three cases during discharge (first 7200 s) and recovery time.

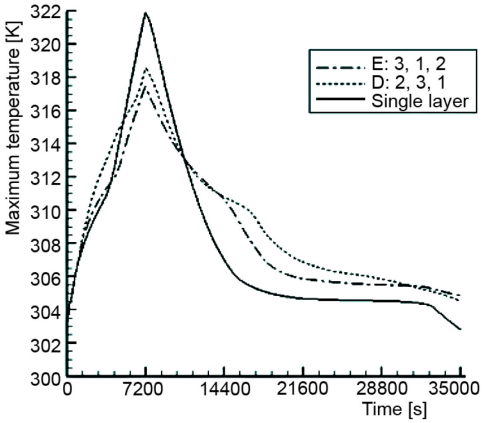

Figure 10. Battery maximum temperature rise during 36000 s for cases E, D, and single layer

The largest gap between battery maximum temperatures for these three cases (from 317 K for case E to 322 K for the single layer) happens in 7200th second. During this two hours' period, a sudden slope change is observed for each case. This slope change for cases D, E and single layer takes place in the time intervals 6200-6600 s, 4200-4800 s, and 3500-4000 s, respectively. This issue is regarded to the increase of the rate of battery's temperature rise which can be justified by considering the liquid fraction graph.

Figure 10 demonstrates that with natural convection as the boundary condition, arrangement E with a maximum temperature of about 317 K after 7200 s is still more preferable than case D. In addition, it is observed that the single layer with maximum temperature of 322 K cannot be useful anymore and the maximum temperature for case D lies between these two values that equals to 318.6 K. As is seen in this figure, in the recovery mode first of all the single layer recovers completely. For two other cases, although case D has a higher maximum temperature in comparing to case E and only at the end of the time period maximum temperature of case E exceeds that of case D, after 36000 s, all the three PCM layers are recovered. Meanwhile, PCM of case E recover after about 41000 s which is because of different thermal conductivities that was explained in the chapter *Results for insulated boundary condition*.

In the following, liquid fraction variations with time after 7200 s are presented for these three arrangements.

In fig. 11, it is disclosed that unlike PCM with insulated walls, in the third layer which is filled with PCM1, phase change initiates just after the start of discharge. This is due to higher ambient temperature than the battery and PCM initial temperature and consequently flowing thermal flux from the ambience to the battery. In addition, it is seen that in about 6500th second all PCM have turned into liquid and cannot play the role of a coolant. This fact reflects its effect by the increased slope in fig. 10.

The liquid fraction graphs for case E are given in fig. 12. As is seen in this figure, after 7200 s unlike the previous arrangements, about 10% of PCM2 located in the inner layer

has not been melted yet. Therefore, the capacity of insensible energy absorption still exists even after the end of discharge mode period.

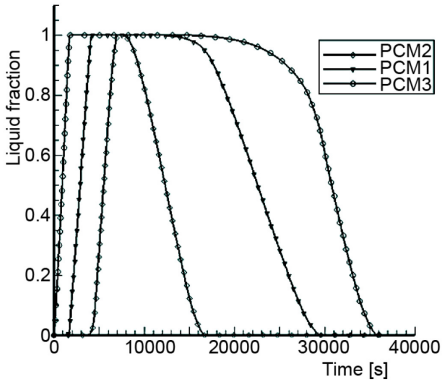

Figure 11. Liquid fraction as a function of time for arrangement D

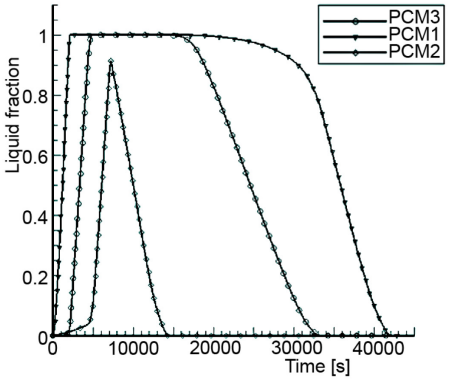

Figure 12. Liquid fraction variations vs. time for arrangement E

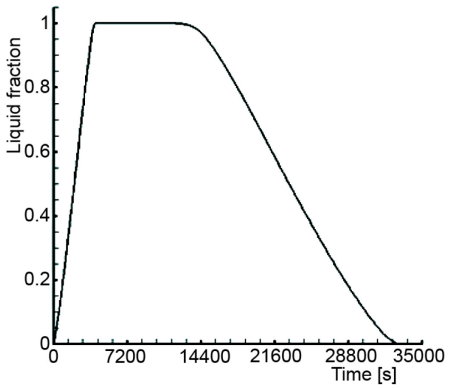

Figure 13. Liquid fraction as a function of time for single layer

In fig. 13 which is plotted for the single layer case, it can be seen that after about 4000 seconds from the beginning of discharge, all the PCM is melted, hence it is not capable of declining the temperature rise inside the battery. Therefore, it can be concluded that the single layer case is not efficient when natural convection is applied at the boundaries.

Figures 10-13 refer to the situation in which convection heat transfer coefficient is considered 35 W/m^2K. In order to abate recovery time, one of effective ways is to use fans to obtain a higher convection heat transfer coefficient. Therefore, the simulation of case D was repeated with h = 130 W/m^2K. The results showed that the recovery time descends about 50%. Another suggestion for more decrease in recovery time is using fins.

Conclusions

The following main conclusions are drawn from this research.

- Considering different thermal conductivities for solid and liquid phases has negligible effect on the results.
- In order to have better cooling in Li-ion batteries within two hours discharge, the single layer case is preferred in comparison with three-layer cases with insulated walls.
- Arrangement E is preferred to the other three-layer arrangements and the single layer case with natural convection boundary during two hours discharge of a Li-ion battery.
- For three-layer cases, the optimum case (the case with the lowest battery maximum temperature after 7200 s discharge) is the one in which PCM with higher thermal conductivi-

ty is placed closer to the battery and PCM with lower thermal conductivity is placed in outer walls.

- If recovery time is also considered as an important factor, decreasing heat resistance in the third PCM layer is essential and one solution can be using fin.

Nomenclature

A – zone constant
C_p – specific heat capacity, [Jkg^{-1}K^{-1}]
g – gravitational acceleration, [ms^{-2}]
H – enthalpy, [Jkg^{-1}]
h – sensible heat, [Jkg^{-1}]
h – convection heat transfer coefficient [Wm^{-2}K^{-1}]
I – stress tensor
k – thermal conductivity, [Wm^{-1}K^{-1}]
L – latent heat, [Jkg^{-1}]
S – source term, [Jm^{-3}s^{-1}]
T – temperature, [K]
t – time, [s]
v – velocity, [ms^{-1}]

Greek symbols

ε – small number (0.001)
β – liquid fraction
μ – viscosity, [kgm^{-1}s^{-1}]
ρ – density, [kgm^{-3}]
$\boldsymbol{\tau}$ – stress tensor

Subscripts

amb – ambient
b – boundary between solid and melted PCM
h – heat
i – initial
m – melting
mush – mushy zone
p – constant pressure
ref – reference
w – wall

Acronym

EV/HEV – electric vehicles/hybrid EV

References

[1] Mills, A., Al-Hallaj, S., Simulation of Passive Thermal Management System for Lithium-Ion Battery Packs, *J.Power Sources, 141* (2005), 2, pp. 307-315
[2] Hajmohammadi, M. R., *et al.*, New Methods to Cope with Temperature Elevations in Heated Segments of Flat Plates Cooled by Boundary Layer Flow, *Thermal Science,* DOI: 10.2298/TSCI130128159H
[3] Hajmohammadi, M. R., *et al.*, Detailed Analysis for the Cooling Performance Enhancement of a Heat Source under a Thick Plate, *Energy Conversion and Management*, *76* (2013), Dec., pp. 691-700
[4] Radhakrishnan, K. B., Balakrishnan, A. R., Heat Transfer Analysis of Thermal Energy Storage using Phase Change Materials, *Heat Recovery Systems and CHP, 12* (1990), 5, pp. 427-435
[5] Kurklu, A., *et al.*, Mathematical Modelling of the Thermal Performance of a Phase-Change Material (PCM) Store: Cooling Cycle, *Applied Thermal Engineering, 16* (1996), 7 pp. 613-623
[6] Domanski, R., Fellah, G., Exergy Analysis for the Evaluation of a Thermal Storage System Employing PCMS with Different Melting Temperatures, *Applied Thermal Engineering, 16* (1996), 11, pp. 907-919
[7] Kurklu, A., Energy Storage Applications in Greenhouses by Means of Phase Change Materials (PCMs): A Review, *Renewable Energy, 13* (1998), 1, pp. 89-103
[8] Zivkovic, B., Fujii, I., An Analysis of Isothermal Phase Change of Phase Change Material within Rectangular and Cylindrical Containers, *Solar Energy, 70* (2001), 1, pp. 51-61
[9] Enibe, S. O., Performance of a Natural Circulation Solar Air Heating System with Phase Change Material Energy Storage, *Renewable Energy, 27* (2002), 1, pp. 69-86
[10] Mahfuz, M. H., *et al.*, Exergetic Analysis of a Solar Thermal Power System with PCM Storage, *Energy Conversion and Management*, *78* (2014), Feb., pp. 486-492
[11] Al-Hallaj, S., Selman, J. R., Thermal Modeling of Secondary Lithium Batteries for Electric Vehicle/Hybrid Electric Vehicle Applications, *Journal of Power Sources*, *110* (2002), 2, pp. 341-348
[12] Al-Hallaj, S., Selman, J. R., A Novel Thermal Management System for Electric Vehicle Batteries Using Phase-Change Material, *J. Electrochemical Society*, *147* (2000), 9, pp. 3231-3236
[13] Alawadhi, E. M., Amon, C. H., Thermal Analysis of a PCM Thermal Control Unit for Portable Electronic Devices: Experimental and Numerical Studies, *Proceedings*, 8th Intersociety Conference on Thermal and Thermomechanical Phenomena in Electronic Systems, San Diego, Cal., USA, 2002, Vol. 26, pp. 116-125

[14] Khateeb, S. A., *et al.*, Design and Simulation of a Lithium-Ion Battery with a Phase Change Material Thermal Management System for an Electric Scooter, *Journal of Power Sources, 128* (2004), 2, pp. 292-307
[15] Ramandi, M. Y., *et al.*, Heat Transfer and Thermal Management of Electric Vehicle Batteries with Phase Change Materials, *Heat and Mass Transfer, 47* (2011), 7, pp. 777-788
[16] Bejan, A., *Heat Transfer*, John Wiley and Sons Inc., New York, USA, 1993

Paper submitted: May 15, 2013
Paper revised: March 5, 2014
Paper accepted: March 22, 2014